Super Fermi polaron and Nagaoka ferromagnetism in a two-dimensional square lattice

Hui Hu,* Jia Wang,† and Xia-Ji Liu‡
Centre for Quantum Technology Theory, Swinburne University of Technology, Melbourne 3122, Australia

(Received 1 December 2023; accepted 30 July 2024; published 13 August 2024)

We consider the Fermi polaron problem of an impurity hopping around a two-dimensional square lattice and interacting with a sea of fermions at given filling factor. When the interaction is attractive, we find standard Fermi polaron quasiparticles, categorized as attractive polarons and repulsive polarons. When the interaction becomes repulsive, interestingly, we observe an unconventional highly excited polaron quasiparticle, sharply peaked at the corner of the first Brillouin zone with momentum $\mathbf{k} = (\pm\pi, \pm\pi)$. This super Fermi polaron branch arises from the dressing of the impurity's motion with holes, instead of particles of fermions. We show that super Fermi polarons become increasingly well defined with increasing impurity-fermion repulsions and might be considered as a precursor of Nagaoka ferromagnetism, which would appear at sufficiently large repulsions and at large filling factors. We also investigate the temperature dependence of super Fermi polarons and find that they are thermally robust against the significant increase in temperature.

DOI: 10.1103/PhysRevA.110.023314

I. INTRODUCTION

The problem of a single impurity moving in a many-body environment of a noninteracting Fermi sea is probably the simplest quantum many-body system [1]. It was first addressed by Landau 90 years ago in a two-page short paper [2], which gives birth to a fundamental concept known as quasiparticle. Termed as a "polaron" quasiparticle, or more specifically "Fermi polaron" to reflect the Fermi sea background, this impurity problem arises in diverse research fields, including Kondo screening [3–5], Anderson' s orthogonality catastrophe [6], the x-ray Fermi edge singularity [7–9], Nagaoka ferromagnetism [10–14], the phase string effect [15], ultracold atomic polaron [16–24], and most recently exciton-polariton polaron in two-dimensional materials [25,26].

Among those fields, the recent research on ultracold atomic polarons attracts particular interests due to the unprecedented tunability and controllability on quantum atomic gases [27]. For instance, the interatomic interaction can be precisely tuned by changing an external magnetic field across a Feshbach resonance [28]. In the strongly interacting regime near resonance, particle-hole excitations of the Fermi sea are attached to the impurity [16], forming an attractive Fermi polaron in the absolute ground state. Moreover, above the Feshbach resonance in the presence of a two-body bound (molecule) state, although the underlying interaction between the impurity and the Fermi sea is always attractive, an additional repulsive Fermi polaron develops as an excited state [14,29]. Over the past 15 years, attractive and repulsive Fermi polarons have been extensively investigated in a quantitative manner, both experimentally [17,18,20,30–32] and theoretically [16,22–24,33–49].

In this work, we would like to suggest the existence of a novel Fermi polaron in two-dimensional (2D) optical lattices, which can be readily realized in cold-atom experiments, again owing to the unprecedented tunability and controllability. In lattices, the interaction between the impurity and fermions in the Fermi sea, as given by the on-site repulsion strength U [see Eq. (1) below], can become positive on the molecular side of the Feshbach resonance since the absolute ground state of molecules can be effectively projected out from the Hilbert space by the lattice potential (i.e., the ground state is too deep to be effectively occupied in the timescale of cold-atom experiments). In addition, the filling factor ν of fermions can be tuned to be near unity ($\nu \sim 1$), so the background environment can be more conveniently described as a new Fermi sea of holes, centered around the corner of the first Brillouin zone [see, i.e., Fig. 1(e)], where $\mathbf{k} = (k_x, k_y) = (\pm\pi, \pm\pi)$. Therefore, the repulsion between the impurity and fermions can be equivalently treated as an effective attraction between the impurity and holes, leading to an "attractive" Fermi polaron that has the *highest* energy. This state is analogous to the highly excited super-Tonk-Girardeau gas phase found in a one-dimensional Bose gas with infinitely strong attraction [50], which is contrasted with a ground-state Tonk-Girardeau gas with infinitely strong repulsions. Thus, it is useful to dub the novel highest-lying Fermi polaron as a *super* Fermi polaron.

We find that the appearance of the super Fermi polaron is a precursor of Nagaoka ferromagnetism [10], which is anticipated to occur at large repulsion and at large filling factor for a cluster of spin-1/2 fermions [11–14]. There, all fermions prefer to align their spin (i.e., into the spin-up state) due to the strong repulsion between two fermions with unlike spin. In other words, if initially we consider a spin-down fermion (i.e., impurity) immersed in a sea of spin-up fermions, the spin-down fermion at zero momentum prefers to flip its spin, occupies into a spin-up state near Fermi surface located at about $\mathbf{k} = (\pm\pi, \pm\pi)$, and eventually creates a fully spin-polarized

*Contact author: hhu@swin.edu.au
†Contact author: jiawang@swin.edu.au
‡Contact author: xiajiliu@swin.edu.au

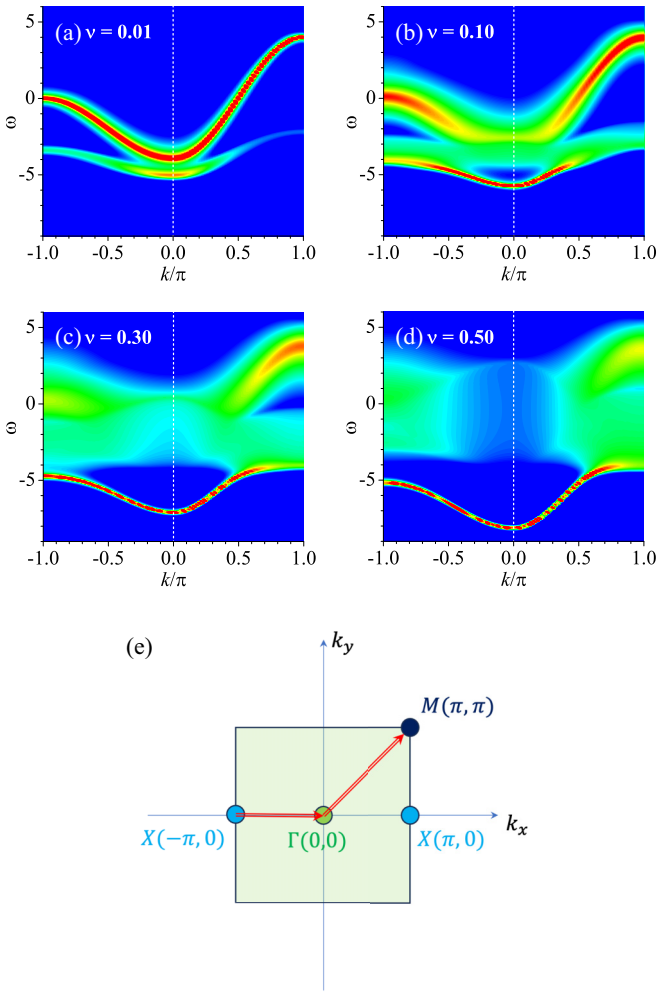

FIG. 1. Impurity spectral function $A(\mathbf{k},\omega)$ at different filling factors ν and at a negative interaction strength $U=-6t$, shown as 2D contour plots with a logarithmic scale in units of t^{-1}. The blue and red colors represent the minimum intensity (i.e., $0.01t^{-1}$) and maximum intensity (i.e., t^{-1}), respectively. On the left-hand side of each panel (i.e., $k<0$), we consider a cut in the first Brillouin zone from the X point $X=(-\pi,0)$ to the Γ point $\Gamma=(0,0)$, as illustrated in the subplot (e), so k represents the wave vector $\mathbf{k}=(k,0)$. On the right-hand side of the dotted line (i.e., $k>0$), the cut is along the diagonal direction from the Γ point to the M point $M=(\pi,\pi)$, so k gives the wave vector $\mathbf{k}=(k,k)$. The energy ω is in units of t and the temperature is set to $k_BT=0.1t$.

noninteracting Fermi sea. In our case of super Fermi polaron, of course, the impurity cannot take spin-flip and automatically turn itself into a fermion. However, this tendency is clearly demonstrated in the impurity spectral function: on the one hand, near zero momentum the quasiparticle peak becomes increasingly blurred in the spectral function; on the other hand, a very sharp peak well develops at $\mathbf{k}=(\pm\pi,\pm\pi)$. To further confirm the instability towards Nagaoka ferromagnetism, at low temperature we calculate the ground-state energy of the super Fermi polaron and find that it is indeed preferable in energy to take an imaginable "spin-flip" at large repulsion.

The rest of the paper is laid out as follows. In Sec. II, we describe the model Hamiltonian for an impurity interacting with a Fermi sea on a 2D square lattice with on-site interaction. In Sec. III, we solve the model Hamiltonian at finite temperature, by using a non-self-consistent many-body T-matrix approach that captures the crucial one-particle-hole excitations of the Fermi sea. In Sec. IV, we first report the results of conventional Fermi polarons with an attractive on-site interaction strength $U<0$. We then consider a repulsive on-site interaction ($U>0$) and discuss the evolution of the impurity spectral function as functions of the filling factor and repulsion strength. We clearly demonstrate the Nagaoka ferromagnetic transition by comparing the energies of the Fermi polaron state and of the fully polarized Fermi sea, and determine the critical interaction strength at a given filling factor. We finally discuss the temperature dependence of Fermi polarons, and show the remarkable thermal robustness of the super Fermi polaron. We conclude in Sec. V and present an outlook for future studies.

II. MODEL HAMILTONIAN

Let us start by considering one impurity and N fermionic atoms moving on a 2D $L\times L$ square optical lattice, with hopping strengths t_d and t, respectively. The impurity interacts with fermions when they occupy the same site only. In momentum space, the system can be described by the standard Hubbard model

$$\mathcal{H}=\sum_{\mathbf{k}}(\xi_{\mathbf{k}}c_{\mathbf{k}}^{\dagger}c_{\mathbf{k}}+E_{\mathbf{k}}d_{\mathbf{k}}^{\dagger}d_{\mathbf{k}})+\frac{U}{A}\sum_{\mathbf{k}\mathbf{k}'\mathbf{q}}c_{\mathbf{k}}^{\dagger}d_{\mathbf{q}-\mathbf{k}}^{\dagger}d_{\mathbf{q}-\mathbf{k}'}c_{\mathbf{k}'}, \quad (1)$$

where $A=(La)^2$ is the area of the system with a lattice spacing a, $c_{\mathbf{k}}^{\dagger}$, and $d_{\mathbf{k}}^{\dagger}$ are the creation field operators for fermionic atoms and the impurity, respectively. The first term of the model Hamiltonian describes the single-particle motion with dispersion relation

$$\xi_{\mathbf{k}}=-2t(\cos k_x+\cos k_y)-\mu \quad (2)$$

for atoms and

$$E_{\mathbf{k}}=-2t_d(\cos k_x+\cos k_y) \quad (3)$$

for the impurity, while the last term is the interaction Hamiltonian with on-site interaction strength U. Here, for convenience we have taken the lattice size $a=1$, so the first Brillouin zone is given by $k_x,k_y\subseteq[-\pi,+\pi]$. We introduce a chemical potential μ to tune the filling factor $\nu=N/A$ of atoms on the lattice. In the thermodynamic limit (i.e., $N\to\infty$), the motion of fermionic atoms is barely affected by the existence of the impurity, so at finite temperature T, the chemical μ simply relates to ν by the noninteracting number equation

$$\nu=\frac{1}{A}\sum_{\mathbf{k}}\langle c_{\mathbf{k}}^{\dagger}c_{\mathbf{k}}\rangle=\int_{-\pi}^{+\pi}\frac{dk_xdk_y}{(2\pi)^2}f(\xi_{\mathbf{k}}), \quad (4)$$

where $f(x)=1/[e^{x/(k_BT)}+1]$ is the Fermi-Dirac distribution function. In contrast, the behavior of the impurity is strongly modified by the on-site interaction and could be solved below by using a non-self-consistent many-body T-matrix theory. Moreover, for a single impurity at finite temperature, the impurity chemical potential tends to infinity ($\mu_{\rm imp}\to-\infty$) due to the vanishing impurity density in the thermodynamic limit. This impurity chemical potential $\mu_{\rm imp}$ can be eliminated, by

shifting the frequency ω with respect to it (i.e., by redefining $\omega + \mu_{\rm imp}$ as ω) [46]. Throughout the work, we always assume the impurity and fermionic atoms have the same hopping strength, i.e., $t_d = t$, and we use t as the units of energy.

III. NON-SELF-CONSISTENT MANY-BODY T-MATRIX APPROACH

The non-self-consistent many-body T-matrix theory of Fermi polarons has been thoroughly studied in the past, without considering optical lattices. The generalization of the theory to the lattice case is straightforward since the resulting equations for the key quantities, such as the vertex function and the impurity self-energy, take the exactly same forms. The only change is to restrict the summation over the momentum $\mathbf{k} = (k_x, k_y)$ to the first Brillouin zone. Therefore, we directly write down the inverse vertex function [33,46]

$$\Gamma^{-1}(\mathbf{q}, \omega) = \frac{1}{U} - \int_{-\pi}^{+\pi} \frac{dk_x dk_y}{(2\pi)^2} \frac{1 - f(\xi_{\mathbf{k}})}{\omega - \xi_{\mathbf{k}} - E_{\mathbf{q}-\mathbf{k}}}, \quad (5)$$

and the impurity self-energy

$$\Sigma(\mathbf{k}, \omega) = \int_{-\pi}^{+\pi} \frac{dq_x dq_y}{(2\pi)^2} f(\xi_{\mathbf{q}-\mathbf{k}}) \Gamma(\mathbf{q}, \omega + \xi_{\mathbf{q}-\mathbf{k}}). \quad (6)$$

Once the impurity self-energy is determined, we calculate the impurity Green's function [33,46]

$$G(\mathbf{k}, \omega) = \frac{1}{\omega - E_{\mathbf{k}} - \Sigma(\mathbf{k}, \omega)}. \quad (7)$$

The emergent Fermi polarons can be well characterized by the impurity spectral function

$$A(\mathbf{k}, \omega) = -\frac{1}{\pi} \mathrm{Im} G(\mathbf{k}, \omega), \quad (8)$$

where the existence of polaron quasiparticles is clearly revealed by a sharp spectral peak. The position and the width of the spectral peak relate to the energy $\mathcal{E}_P(\mathbf{k})$ and the decay rate (i.e., inverse lifetime) $\Gamma_P(\mathbf{k})$ of polaron quasiparticles [29,33], respectively. It is readily seen that the polaron energy $\mathcal{E}_P(\mathbf{k})$, of either attractive Fermi polaron or repulsive Fermi polaron, is given by the pole of the impurity Green's function, if we take the replacement $\omega \to \mathcal{E}_P(\mathbf{k})$:

$$\mathcal{E}_P(\mathbf{k}) = E_{\mathbf{k}} + \mathrm{Re}\Sigma[\mathbf{k}, \mathcal{E}_P(\mathbf{k})]. \quad (9)$$

By Taylor-expanding the impurity self-energy around the polaron energy, i.e.,

$$\Sigma(\omega) \simeq \mathrm{Re}\Sigma(\mathcal{E}_P) + \frac{\partial \mathrm{Re}\Sigma(\omega)}{\partial \omega}(\omega - \mathcal{E}_P) + i\mathrm{Im}\Sigma(\mathcal{E}_P), \quad (10)$$

where we suppress the dependence of the impurity self-energy on the momentum $\mathbf{k}$, the impurity spectral function takes an approximate Lorentzian form in the vicinity of the polaron energy

$$A(\mathbf{k}, \omega) \simeq \frac{\mathcal{Z}_{\mathbf{k}}}{\pi} \frac{\Gamma_P(\mathbf{k})/2}{[\omega - \mathcal{E}_P(\mathbf{k})]^2 + \Gamma_P^2(\mathbf{k})/4}. \quad (11)$$

Here, $\mathcal{Z}_{\mathbf{k}}$ is the polaron residue

$$\mathcal{Z}_{\mathbf{k}} = \left[1 - \frac{\partial \mathrm{Re}\Sigma(\mathbf{k}, \omega)}{\partial \omega}\Big|_{\omega = \mathcal{E}_P(\mathbf{k})}\right]^{-1}, \quad (12)$$

and $\Gamma_P(\mathbf{k})$ is the polaron decay rate

$$\Gamma_P(\mathbf{k}) = -2\mathcal{Z}_{\mathbf{k}} \mathrm{Im}\Sigma[\mathbf{k}, \mathcal{E}_P(\mathbf{k})]. \quad (13)$$

In the dilute limit of vanishingly small filling factor $\nu \to 0$, where the interesting physics occurs at the very small momentum, the system behaves like an interacting Fermi gas in free space with a contact interaction potential. In this case, for a negative on-site interaction strength $U < 0$ and an associated binding energy ε_B, we may then introduce a dimensionless interaction parameter

$$\zeta = \tfrac{1}{2} \ln(2\varepsilon_F/\varepsilon_B) \quad (14)$$

to fully characterize the universal low-energy polaron physics [35,39].

It should be noted that, at zero temperature our non-self-consistent many-body T-matrix theory is fully equivalent to a variational Chevy ansatz [14], which has been extensively used in the investigations of Nagaoka ferromagnetism [11–13], particularly for the idealized case of infinitely large repulsion ($U \to +\infty$). Thus, our work might be viewed as a useful extension of these variational studies to the realistic cases with large but finite repulsion at nonzero temperature.

The key difficulty of applying the non-self-consistent T-matrix theory for Fermi polarons comes from the numerical integration over the momentum $\mathbf{k}$ in Eq. (5). This is caused by the singularity in the integrand, which occurs when the energy or frequency ω lies in the two-particle scattering continuum, i.e., $\omega = \xi_{\mathbf{k}} + E_{\mathbf{q}-\mathbf{k}}$, at certain momenta $\mathbf{k}$. A formal procedure to solve the difficulty is to first calculate the imaginary part of the vertex function

$$\mathrm{Im}\Gamma^{-1}(\mathbf{q}, \omega) = \frac{\pi}{A} \sum_{\mathbf{k}} [1 - f(\xi_{\mathbf{k}})] \delta(\omega - \xi_{\mathbf{k}} - E_{\mathbf{q}-\mathbf{k}}), \quad (15)$$

where $\delta(x)$ is the Dirac delta function [46]. We then use the Kramers-Kronig relation to recover the real part of the vertex function. In our case, since the momentum is restricted to the first Brillouin zone, a more economic and straightforward way is to introduce a nonzero broadening factor η and replace the frequency ω with $\omega + i\eta$ to remove the singularity of the integrand. We then extrapolate the results to the zero-broadening limit. In practice, we find the following linear extrapolation with a broadening factor $\eta = 0.3t$,

$$\Gamma^{-1}(\mathbf{q}, \omega) \simeq 2\Gamma^{-1}(\mathbf{q}, \omega + i\eta) - \Gamma^{-1}(\mathbf{q}, \omega + 2i\eta), \quad (16)$$

works very well. The choice of the value $\eta = 0.3t$ is discussed in Appendix.

IV. RESULTS AND DISCUSSIONS

A. Fermi polarons at $U < 0$

Let us first consider the cases with negative on-site interaction strengths $U < 0$, which connect to the well-studied 2D Fermi polarons in free space [19,35,37]. These cases have also been investigated by using an *ab initio* impurity lattice Monte Carlo method [39]. However, the *ab initio* results are restricted to the polaron energy only.

In Fig. 1, we present the impurity spectral function at $U = -6t$ and at four filling factors (as indicated), in the form of a 2D contour plot with a logarithmic scale, where the spectral

peaks in red color can be clearly identified. To account for the anisotropy of the first Brillouin zone, in each panel, following the convention we consider two cuts on the Brillouin zone along the ΓX line (see the left part) and the ΓM line (the right part). As the filling factor ν increases, we always find two branches in the spectral function: the low-energy attractive Fermi polarons and high-energy repulsive Fermi polarons. However, the evolutions of the two kinds of Fermi polarons as a function of the filling factor turn out be very different.

For the very-low filling factor $\nu = 0.01$ in Fig. 1(a), the spectral function is dominated by the repulsive polaron branch whose energy is always larger than $-4t_d = -4t$ (which is the lowest single-particle energy of the impurity since we take $t_d = t$). The attractive polaron branch is only visible at low momentum $\mathbf{k} \sim 0$. Towards the X point or the M point, the spectral weight of attractive Fermi polarons quickly disappears. This weak attractive polaron branch might be understood from the results of 2D Fermi polarons in free space. In the dilute limit at zero temperature, the dispersion relation of fermionic atoms can be well approximated as

$$\xi_{\mathbf{k}} \simeq t\mathbf{k}^2 - (\mu + 4t) = \frac{\hbar^2\mathbf{k}^2}{2m} - \varepsilon_F, \tag{17}$$

where $m = \hbar^2/(2t)$ is the effective mass and $\varepsilon_F = \hbar^2 k_F^2/(2m)$ is the Fermi energy with Fermi wave vector $k_F = (4\pi\nu)^{1/2}$. It is easy to see that $\varepsilon_F = 4\pi\nu t$. At $U = -6t$, the binding energy $\varepsilon_B \sim t$. Thus, the dimensionless interaction parameter in Eq. (14) is about $\zeta \sim (1/2)\ln(8\pi\nu) \simeq -0.7$, which is very close to the threshold for the polaron-molecule transition [35,39]. At this interaction parameter, the residue $\mathcal{Z}_{\mathbf{k}\sim 0}$ for the attractive polaron is not significant.

For the low filling factor $\nu = 0.1$ in Fig. 1(b), the dimensionless interaction strength ζ increases to about $\zeta \sim 0.5$, where near-zero momentum the attractive Fermi polaron is well defined. Indeed, we find that a much sharper attractive polaron peak with large spectral weight or polaron residue $\mathcal{Z}_{\mathbf{k}}$. Accordingly, the repulsive polaron peak near zero momentum becomes blurred, with much smaller spectral weight. Interestingly, the repulsive Fermi polaron at large momentum near the X point or the M point remains sharply peaked. This observation is in marked contrast to the free space 2D polaron model, where Fermi polarons always become less well defined at large momentum. Therefore, this feature should be related to the unique structure of square lattice. We may understand it as a consequence of the van Hove singularity is in the density of states of square lattice. In particular, the logarithmically divergent density of states at the X point could be energetically favorable for particle-hole excitations and therefore leads to more stable Fermi polarons. On the other hand, a well-marked repulsive polaron at the M point seems to indicate a more robust two-body bound state at the corner Brillouin zone than at zero momentum. To better show the robust repulsive Fermi polaron, we also report in Fig. 2 the evolution of the one-dimensional spectral function as the momentum increases along the ΓM line.

As we further increase the filling factor ν, the effect the square lattice band structure becomes more prominent. As shown in Figs. 1(c) and 1(d) for $\nu = 0.3$ and $\nu = 0.5$, the spectrum of the upper repulsive Fermi polaron distributes much wider, in sharp contrast to the attractive Fermi polaron whose spectral response becomes increasingly narrower. Nevertheless, at the filling factor as large as $\nu = 0.3$, the repulsive polaron peak near the M point remains visible, although the spectral weight of the repulsive branch gets strongly depleted close to the Γ point at zero momentum.

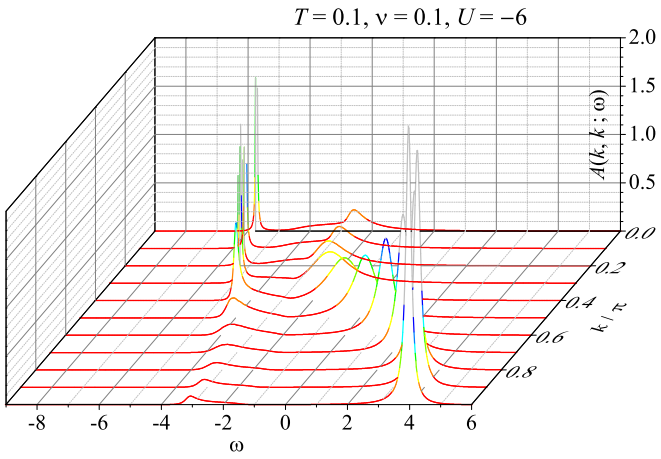

FIG. 2. Impurity spectral function $A(k_x = k, k_y = k; \omega)$ along the diagonal direction of the first Brillouin zone [i.e., the ΓM line in Fig. 1(e)], at temperature $k_B T = 0.1t$, filling factor $\nu = 0.1$, and a negative interaction strength $U = -6t$. The energy ω and the spectral function $A(\mathbf{k}, \omega)$ are in units of t and t^{-1}, respectively.

To better understand the robust repulsive Fermi polaron near the M point, we focus on the case $\nu = 0.1$ and report in Fig. 3(a) the real part of the inverse impurity green function

$$\mathrm{Re}G^{-1}(\mathbf{k}, \omega) = \omega - E_{\mathbf{k}} - \mathrm{Re}\Sigma(\mathbf{k}, \omega) \tag{18}$$

at three different momenta. The condition of a pole in the impurity green function, i.e., $\mathrm{Re}G^{-1}(\mathbf{k}, \omega) = 0$, determines the polaron energy. We observe that although in general $\mathrm{Re}G^{-1}(\mathbf{k}, \omega)$ increases with the frequency ω, it has a peculiar peak-dip structure around the bottom of the energy band (i.e., $\omega \sim -4t$ at zero momentum). The depth of this peak-dip structure increases with increasing momentum. At $\mathbf{k} = 0$, we find two solutions of $\mathrm{Re}G^{-1}(\mathbf{k}, \omega) = 0$, giving rise to an attractive Fermi polaron at $\omega \simeq -6t$ and a repulsive Fermi polaron at $\omega \simeq -3t$. At $\mathbf{k} = (\pi/2, \pi/2)$ and at the M point with $\mathbf{k}_M = (\pi, \pi)$, the peak values of $\mathrm{Re}G^{-1}(\mathbf{k}, \omega)$ become negative, implying the absence of the attractive polaron. However, the repulsive Fermi polaron always appears, owing to the positive and k-independent slope with increasing frequency.

The existence of repulsive Fermi polaron is generally related to a two-body molecule bound state. In Fig. 3(b), we present the molecule spectral function

$$A_{\mathrm{mol}}(\mathbf{q}, \omega) = -\frac{1}{\pi}\mathrm{Im}\Gamma(\mathbf{q}, \omega), \tag{19}$$

along the ΓM line in the form of a 2D contour plot. We may clearly identify the two-particle scattering continuum enclosed by $\omega_{\min}(\mathbf{q}) = \min_{\{\mathbf{k}\}}(\xi_{\mathbf{k}} + E_{\mathbf{q}-\mathbf{k}})$ and $\omega_{\max}(\mathbf{q}) = \max_{\{\mathbf{k}\}}(\xi_{\mathbf{k}} + E_{\mathbf{q}-\mathbf{k}})$. There is always an in-medium molecule bound state with energy $\mathcal{E}_M(\mathbf{q})$, as revealed by a strong spectral peak near the bottom of the scattering continuum. The dispersion of $\mathcal{E}_M(\mathbf{q})$ is nonmonotonic and exhibits a minimum

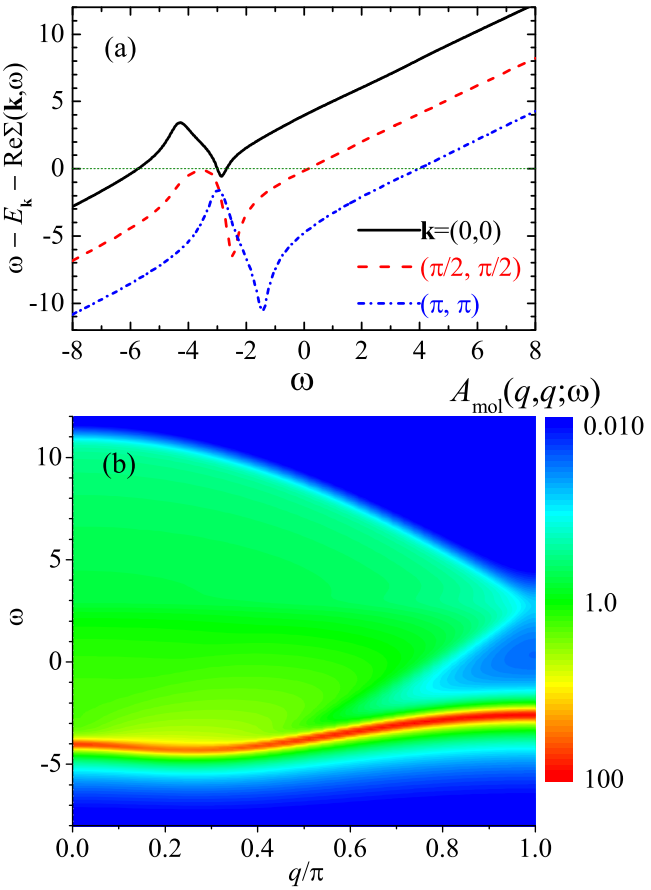

FIG. 3. (a) The real part of the inverse of the impurity Green's function $\mathrm{Re}G^{-1}(\mathbf{k},\omega)$ as a function of the energy ω, at three different wave vectors on the ΓM line in Fig. 1(e): the Γ point (black solid line), $\mathbf{k}=(\pi/2,\pi/2)$ (red dashed line), and the M point (blue dot-dashed line). The pole of the impurity Green's function, at which $\omega - E_{\mathbf{k}} - \Sigma(\mathbf{k},\omega) = 0$ as given by the crossing point with the green dotted line, determines the energy of polaron quasiparticles. (b) The molecular spectral function $A_{\mathrm{mol}}(q_x = q, q_y = q;\omega)$ along the diagonal direction in momentum space, in arbitrary units (as indicated by the color bar in the logarithmic scale). Here, we take the same parameters for T, ν and U as in Fig. 2.

at about $q \sim 0.3\pi$. More importantly, at $q < q_c \sim \pi/2$, the molecule state is buried in the scattering continuum, so the molecule peak has a finite spectral width due to scattering and can be viewed as a quasibound state. Above q_c, the molecule state develops into a true long-lived bound state, although there is a residual spectral width due to thermal broadening. Near the M point, therefore the molecule state becomes very robust. This robustness directly leads to the well-defined repulsive Fermi polaron at the corner of the first Brillouin zone, as we highlighted earlier.

B. Super Fermi polarons at $U > 0$

We now turn to consider a positive on-site interaction $U > 0$. In Fig. 4, we show the 2D contour plots of spectral function at $U = +6t$ and at three filling factors, $\nu = 0.5$ [Fig. 4(a)], $\nu = 0.7$ [Fig. 4(b)], and $\nu = 0.9$ [Fig. 4(c)]. Due to the repulsion, the spectral weight appears only at $\omega > -4t$, when the energy ω is larger than the lowest single-particle energy of the impurity $-4t$. As in the cases of negative on-site interactions, we may identify the existence of two polaron branches in the spectrum. However, these two branches seem to behave very differently from the negative-U case.

First, the low-lying polaron branch always has a notable spectral width and the width increases with increasing filling factor. This is remarkably different from the case with $U < 0$, where the width of the sharply peaked low-lying attractive Fermi polarons is negligible as we increase the filling factor ν above 0.1. Second, the high-lying polaron branch behaves like a well-defined δ-function peak near the M point, regardless of the filling factor. Finally, at large filling factor, i.e., $\nu = 0.9$, the two branches tend to connect with each other.

Therefore, in comparison with the negative-U case, the low-lying and high-lying polaron branches seem to exchange their roles: the low-lying branch behaves more or less like a repulsive Fermi polaron; instead the high-lying branch looks like an attractive Fermi polaron, although it is now restricted to the vicinity of the M point. This exchange in role becomes much more evident when we increase the on-site repulsion. In Fig. 5, we show the impurity spectral function at $U = +12t$ and at the filling factor $\nu = 0.5$. The two polaron branches, both in the one-dimensional plot [Fig. 5(a)] and in the 2D contour plot [Fig. 5(b)], are now clearly separated. In particular, the sharply peaked high-lying polaron branch extends from the M point to the Γ point. Moreover, the high-lying branch at the X point also becomes well defined.

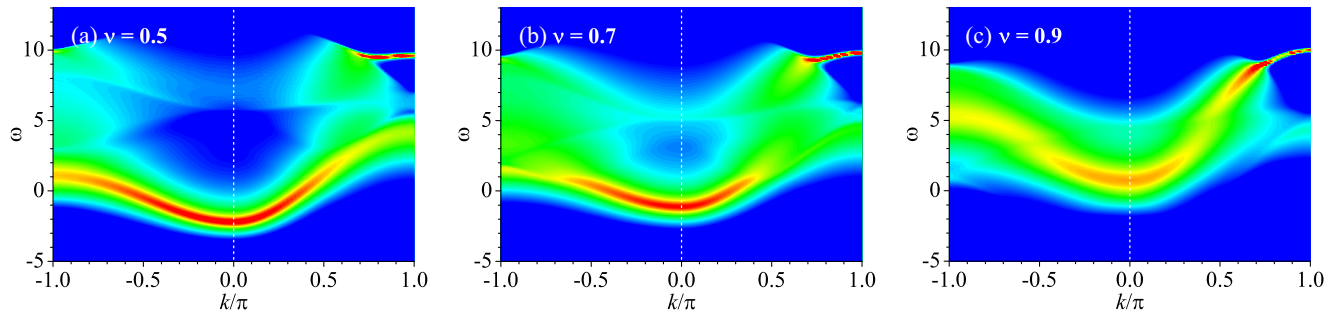

FIG. 4. Impurity spectral function $A(\mathbf{k},\omega)$ at three filling factors (a) $\nu = 0.5$, (b) $\nu = 0.7$, and (c) $\nu = 0.9$, and at a positive interaction strength $U = 6t$. The same logarithmic contour plots as in Fig. 1 are used. On the left-hand side of each panel (i.e., $k < 0$), k represents the wave vector $\mathbf{k} = (k, 0)$ along the $X\Gamma$ line, as illustrated in Fig. 1(e). On the right-hand side (i.e., $k > 0$), k represents the wave vector $\mathbf{k} = (k, k)$ along the ΓM line. The temperature is set to $k_B T = 0.1t$.

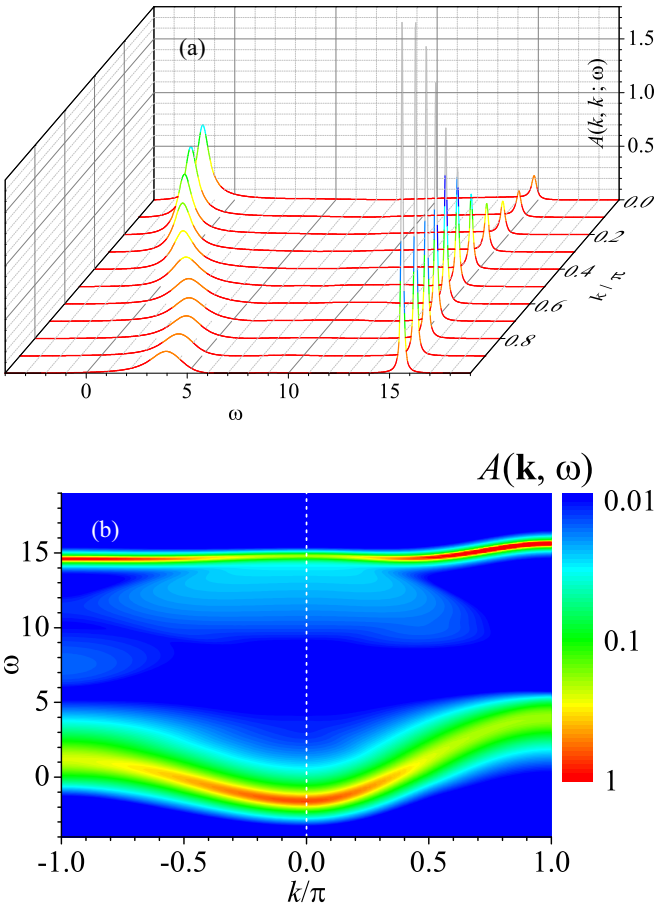

FIG. 5. Impurity spectral function $A(\mathbf{k}, \omega)$ at a large positive interaction strength $U = 12t$, where the upper branch of super Fermi polarons becomes well defined for all wave vectors. In (a) or (b), we show the spectral function in either the standard one-dimensional plot along the diagonal direction $k_x = k_y = k$ [see the ΓM line in Fig. 1(e)] or in the 2D contour plot with a logarithmic scale, where the wave vector $\mathbf{k}$ moves first along the $X\Gamma$ line and then along the ΓM line. In the 2D contour plot, the blue and red colors represent the minimum intensity (i.e., $0.01t^{-1}$) and maximum intensity (i.e., t^{-1}), respectively. The parameters $k_BT = 0.1t$ and $\nu = 0.5$ are used.

The role exchange is mostly easily understood by considering a particle-hole transformation for fermionic atoms. At large filling factor above the half-filling, i.e., $\nu \geqslant 0.5$, it is more convenient to adopt a viewpoint of holes. We treat unoccupied single-particle states as holes and introduce the hole creation field operator $h^\dagger_{\mathbf{k}} = c_{-\mathbf{k}}$. When it acts on a fully occupied Fermi sea with unity filling factor $\nu = 1$ (i.e., the vacuum state of holes), it destroys a fermionic atom with momentum $-\mathbf{k}$ and creates a hole with momentum $\mathbf{k}$. In the hole representation, the interaction Hamiltonian in Eq. (1) can be casted into

$$\mathcal{H}_{\rm int} = U \sum_{\mathbf{k}} d^\dagger_{\mathbf{k}} d_{\mathbf{k}} - \frac{U}{A} \sum_{\mathbf{k}\mathbf{k}'\mathbf{q}} h^\dagger_{\mathbf{k}} d^\dagger_{\mathbf{q}-\mathbf{k}} d_{\mathbf{q}-\mathbf{k}'} h_{\mathbf{k}'}. \qquad (20)$$

Thus, the impurity up-shifts its dispersion relation by an amount U due to the (mean-field) repulsion of the fully occupied Fermi sea, and more importantly, the effective interaction between the impurity and holes becomes attractive, i.e.,

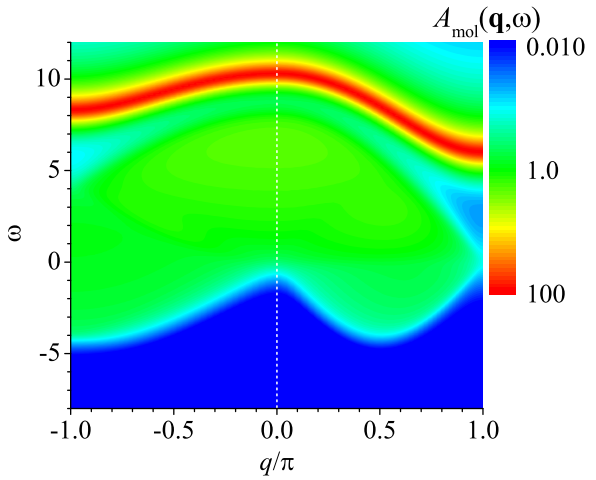

FIG. 6. The molecular spectral function $A_{\rm mol}(\mathbf{q}, \omega)$ at a large positive interaction strength $U = 12t$, in arbitrary units (as indicated by the color map in the logarithmic scale). For $q < 0$, the wave vector $\mathbf{q} = (q, 0)$, while for $q > 0$, we consider the wave vector $\mathbf{q} = (q, q)$ along the diagonal direction. Here, we take the same temperature $k_BT = 0.1t$ and filling factor $\nu = 0.5$ as in Fig. 5.

$U_{\rm eff} = -U < 0$. It is reasonable to assume that this effective attraction would induce attractive Fermi polarons. As the holes occupy around the M point with a smaller hole Fermi sea, the density fluctuation (in the form of particle-hole excitations of the new hole Fermi sea) will first create attractive Fermi polarons around the M point and then extends to the Γ point.

These attractive polarons are highly nontrivial, in the sense that they are the highest in energy but remain completely undamped at zero temperature. It would be useful to name such high-lying Fermi polarons as super Fermi polarons, to highlight the fact that they are *exact* many-body states of the system. In contrast, the usual excited Fermi polaron state, such as repulsive Fermi polaron in the negative-U case, consists of a bundle of many-body states and hence has an intrinsic decay rate even at zero temperature [26,51]. We note that a similar terminology has been used to characterize the highest excited many-body state, i.e., super-Tonk-Girardeau state, in a strongly attractive Bose gas [50].

The effective attraction between the impurity and holes may also lead to a two-body bound state, i.e., a *repulsively* bound pair between the impurity and fermionic atoms due to repulsion. Actually, such a repulsion-induced bound pair has already been experimentally observed in a Bose gas in optical lattices [52]. To confirm the (repulsively) bound pair of the impurity and holes due to the effective attraction $U_{\rm eff}$, we show in Fig. 6 the molecule spectral function along the ΓM line (see the right part of the figure) and the ΓX line (the left part), at the same parameters as in Fig. 5. We see clearly the molecule peak above the two-particle scattering continuum. Analogous to the negative-U case, where a two-body bound state implies the existence of repulsive Fermi polarons, it is natural to classify the low-lying polaron branch in Fig. 5 as repulsive Fermi polarons. In this way, it is not a surprise to find a nonzero decay rate of low-lying polaron branch, even at temperatures close to the zero temperature (i.e., $k_BT = 0.1t$).

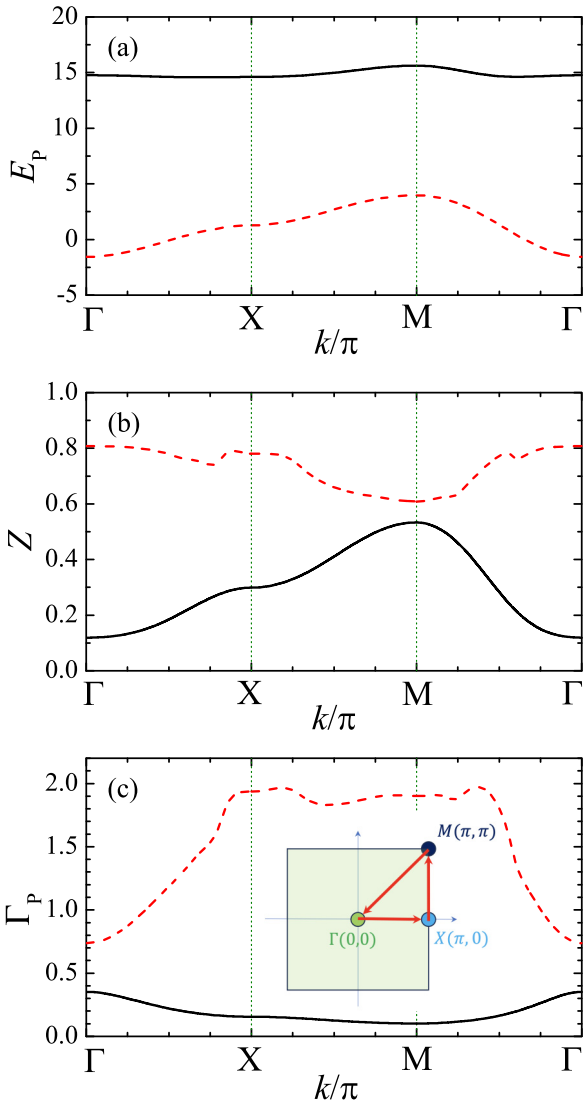

FIG. 7. Quasiparticle properties of Fermi polarons at the positive interaction strength $U = 12t$: (a) polaron energy, (b) residue, and (c) decay rate. Both polaron energy and decay rate are measured in units of t. The black solid lines show the results of the upper branch, super Fermi polarons. The red dashed lines show the properties of the lower branch of standard Fermi polarons. As shown in the inset of (c), along the ΓX line and the XM line, we individually increase k_x and k_y from 0 to π, respectively; while along the $M\Gamma$ line, we decrease both k_x and k_y from π to zero. Once again, we use the temperature $k_B T = 0.1t$ and filling factor $\nu = 0.5$ as in Fig. 5.

The decay rate or spectral broadening of the repulsive Fermi polaron is due to the scattering with fermionic atoms or holes since the repulsive polaron energy is within the two-particle scattering continuum, although the repulsive polaron turns out to be the low-energy, ground-state-like polaron quasiparticle.

For completeness, in Figs. 7(a) to 7(c) we report the polaron energy, residue, and decay rate of both polaron branches along the $\Gamma - X - M - \Gamma$ cut lines, at the same parameters as in Fig. 5. The results of super Fermi polarons and of repulsive Fermi polarons are shown by the solid lines and dashed lines, respectively. We find that the dispersion relation of super Fermi polarons is rather flat, compared with that of repulsive Fermi polarons, indicating a large effective mass. In particular, the effective mass of super Fermi polarons at the M point is negative. This is easy to understand, if we recall the fact that the original mass of the impurity at the M point (i.e., the top of its energy band) is negative. On the other hand, for the parameters we choose, super Fermi polarons always have less spectral weight than repulsive Fermi polarons, as we infer from the polaron residue. Their weights are only comparable at the M point, where super Fermi polarons seem to have the strongest presence. Finally, as we already emphasized, super Fermi polarons have the smallest decay rate at the M point only due to thermal broadening. Repulsive Fermi polarons instead always show a larger decay rate, even at the Γ point, where it is supposed to be most stable.

C. Nagaoka ferromagnetism

At large on-site repulsion, the polaron problem under investigation could be related to the celebrated Nagaoka ferromagnetism in a cluster of spin-1/2 fermions [10], which concerns the instability of a ferromagnetic state with full spin polarization against a single spin flip. Previous variational studies suggest the breakdown of Nagaoka ferromagnetism below a certain critical fermion filling factor ν_c or above a corresponding critical hole filling factor $\delta_c = 1 - \nu_c$ [11–14]. At infinitely large repulsion $U = +\infty$, the simple Chevy ansatz predicts $\nu_c \simeq 0.59$ or $\delta_c \simeq 0.41$ at zero temperature [12,14].

We may treat the impurity as a single spin-down fermions and all the others atoms in the Fermi sea as the spin-up fermions. Thus, at large on-site repulsion U and at large filling factor $\nu > \nu_c(U)$, we may anticipate a phase transition towards the Nagaoka ferromagnetic state, if we allow the impurity to flip its imaginable spin and to jump from the zero momentum spin-down state to a single-particle spin-up state with a momentum $\mathbf{k} \sim \mathbf{k}_F \sim (\pm\pi, \pm\pi)$. Accordingly, the Fermi sea will shuffle its Fermi surface to satisfy the momentum conservation. This anticipation reasonably agrees with the filling factor ν dependence of both Fermi polaron branches at large repulsion $U \gg t$, as we observe in Fig. 4. As the filling factor increases, the tendency of the spin reversal makes low-lying repulsive Fermi polarons less well defined and at the same time makes high-lying super Fermi polarons much more sharply peaked. Thus, in the thermodynamic limit, upon infinitesimal fluctuations in temperature and lattice potential, the fragile low-lying repulsive polaron state can easily turn into a state, where a super Fermi polaron with momentum $\mathbf{k} \sim \mathbf{k}_F$ gains notable weight. As the super Fermi polaron might be viewed as the Nagaoka ferromagnetic state after the imaginable spin-flip, there is a thermodynamic instability of turning the low-lying repulsive polaron state into the Nagaoka ferromagnetic state, if the spin-reversal is allowed.

As a quantitative measure, we may consider the lowest energy of the repulsive Fermi polaron at the Γ point, and compare it to the chemical potential μ, which can be regarded as the energy of the spin-up state after the imaginable spin flip. The stability of the Nagaoka ferromagnetic state is then ensured by the condition, $\mathcal{E}_P(0) > \mu$. Although the repulsive Fermi polaron is not a single quantum many-body state, we believe that this condition could provide a reasonable

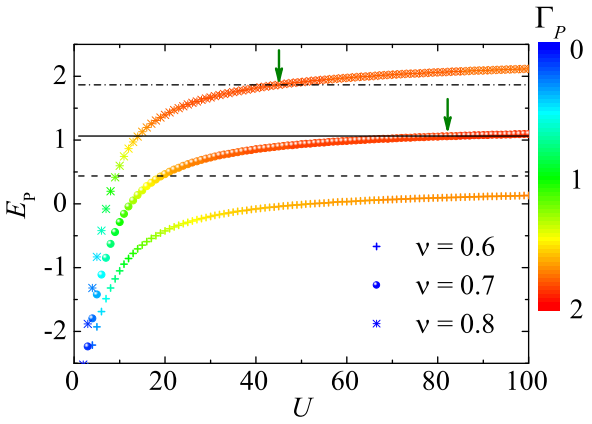

FIG. 8. Zero-momentum polaron energy $\mathcal{E}_P(\mathbf{k} = \mathbf{0})$ as a function of the positive interaction strength U, with increasing filling factor: $\nu = 0.6$ (plus symbols), $\nu = 0.7$ (circles), and $\nu = 0.8$ (stars). The color of symbols represents the polaron decay rate Γ_P in units of t, as indicated by the color bar. From bottom to top, the three horizontal lines show the chemical potential μ of the Fermi sea at $\nu = 0.6$, $\nu = 0.7$, and $\nu = 0.8$, respectively. The two green arrows indicate the critical interaction strength for Nagaoka ferromagnetism, $U_c \simeq 84t$ at $\nu = 0.7$ and $U_c \simeq 45t$ at $\nu = 0.8$, at which $\mathcal{E}_P(\mathbf{0}) = \mu$. Here, we take the temperature $k_BT = 0.1t$.

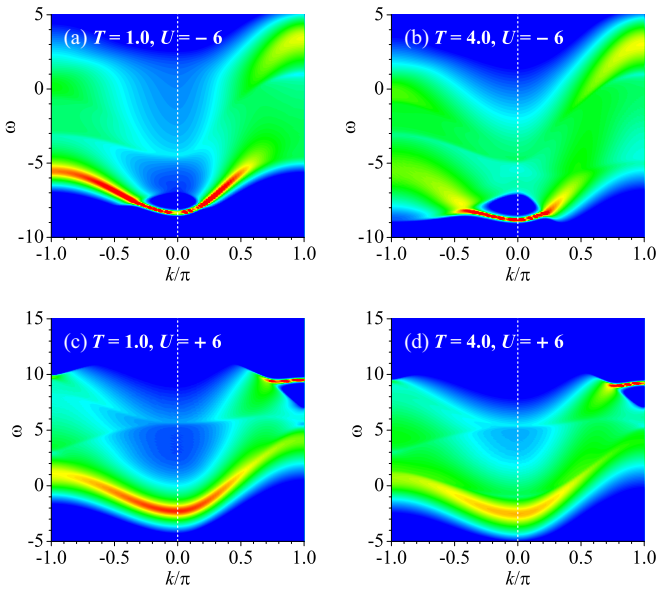

FIG. 9. Impurity spectral function $A(\mathbf{k}, \omega)$ at large temperatures (a), (c) $k_BT = t$ and (b), (d) $k_BT = 4t$. Here, the wave vector $\mathbf{k}$ moves first along the $X\Gamma$ line [i.e., $\mathbf{k} = (k, 0)$] and then along the ΓM line [i.e., $\mathbf{k} = (k, k)$], as illustrated in Fig. 1(e). The upper panel and low panel report the results at $U = -6t$ and $U = +6t$, respectively. We use the same logarithmic contour plots as in Fig. 1 and consider the half-filling of the Fermi sea $\nu = 0.5$.

thermodynamic evaluation of the critical on-site repulsion at a given filling factor, $U_c(\nu)$, at very low temperature.

In Fig. 8, we compare the low-lying repulsive polaron energy $\mathcal{E}_P(0)$ with the chemical potential μ with increasing on-site repulsion, at three filling factors as indicated. At $\nu = 0.6$, we always find that the polaron energy is below the chemical potential, indicating the absence of the Nagaoka ferromagnetic state at the on-site repulsion considered in the figure. This is understandable since $\nu = 0.6$ is very close to the critical filling factor $\nu_c \simeq 0.59$ at $U = +\infty$. The small but nonzero temperature $k_BT = 0.1t$ used in our calculations effectively reduce the interaction effect and may already wash out the Nagaoka ferromagnetism transition. In contrast, at other two filling factors in the figure, by using the criterion $\mathcal{E}_P(0) = \mu$ we find $(W/U)_c \simeq 0.10$ at $\nu = 0.7$ and $(W/U)_c \simeq 0.18$ at $\nu = 0.8$, where $W = 8t$ is the energy bandwidth of the square lattice. These two critical values $(W/U)_c$ agree qualitatively well with the initial estimation by Shastry, Krishnamurthy, and Anderson [11], and the improved variational result by von der Linden and Edwards [13].

D. Finite-temperature effect

We finally briefly discuss the temperature effect. In Fig. 9, we show the 2D contour plot of spectral function at the temperature $T = t$ [see Figs 9(a) and 9(c) on the left] and $T = 4t$ [Figs. 9(b) and 9(d)]. We focus on a filling factor $\nu = 0.5$ and consider both on-site attractions $U = -6t$ (see the upper panel) and repulsions $U = +6t$ (the low panel). We observe that the conventional attractive Fermi polarons in the negative-U case significantly changes with increasing temperature. Quite differently, super Fermi polarons near the M point with on-site repulsions appear to be insensitive to temperature and hence are thermally robust. They remains sharply peaked at the temperature as large as the half-energy bandwidth (i.e., $k_BT = 4t = W/2$).

V. CONCLUSION AND OUTLOOKS

In conclusion, we investigated the Fermi polaron problem in two-dimensional square lattices at finite temperature, with both on-site attractive interactions and repulsive interactions between an impurity and a Fermi sea of noninteracting fermions. The standard non-self-consistent many-body T-matrix approach has been used, which well describes the key ingredient of polaron physics, i.e., the one-particle-hole excitations of the Fermi sea as excited by the on-site interaction [33,46]. This method is equivalent to a variational ansatz previously used to address Nagaoka ferromagnetism [10] of a cluster of spin-1/2 fermions on square lattices [11–14]. However, our diagrammatic calculations are able to obtain the impurity spectral function at finite temperature, thereby leading to new understanding to the old research topic of Nagaoka ferromagnetism.

For on-site attractions at small filling factor, we found conventional Fermi polarons, including both attractive and repulsive branches. In the dilute limit of vanishingly small filling factor, the results can be well understood by using a free-space Fermi polaron model [35,37,39]. We demonstrated how the polaron physics is affected by the lattice structure. In particular, we showed that the repulsive Fermi polaron at the M point, where $\mathbf{k}_M = (\pm\pi, \pm\pi)$, is relatively robust with increasing filling factor due to the stable two-body bound state at the corner of the first Brillouin zone.

For on-site repulsions at large filling factor, we have found a novel type of Fermi polarons, the so-called super Fermi

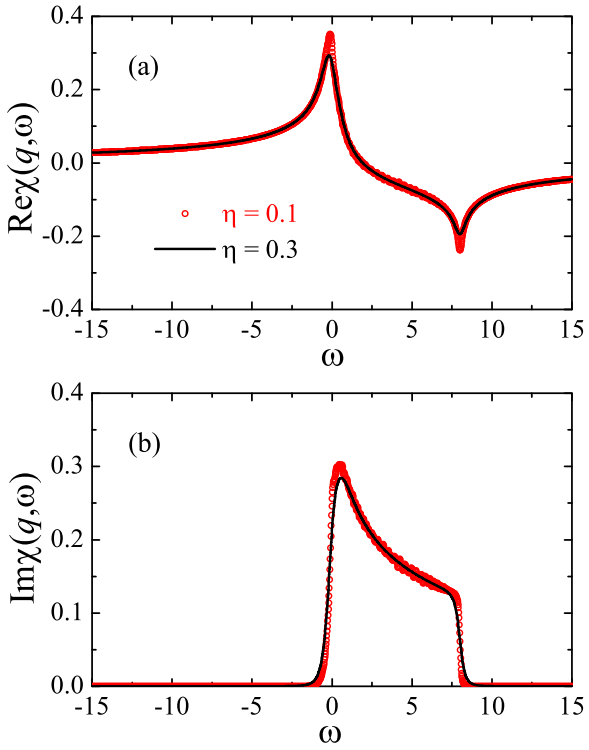

FIG. 10. The real part and imaginary part of the pair propagator $\chi(\mathbf{q}, \omega)$ at zero wave vector $\mathbf{q} = \mathbf{0}$, in arbitrary units. The black lines and red circles show the results with $\eta = 0.3t$ and $\eta = 0.1t$, respectively. The temperature is set to $k_B T = 0.1t$.

polaron, when the repulsion is strong enough. The super Fermi polaron is an exact many-body state centered around the M point and is therefore long-lived at low temperature, although it is highly excited with large energy. We explained that the formation mechanism of high-lying super Fermi polarons is due to an effective attraction between the impurity and holes arising from strong on-site repulsions. Therefore, it can be understood in terms of conventional attractive Fermi polarons. We showed that there is also a ground-state-like, low-lying Fermi polaron branch with on-site repulsion. However, this low-lying polaron branch has a finite decay rate and should be understood as conventional repulsive polarons.

The classification of the two polaron branches in the case of on-site repulsions suggests that the appearance of the super Fermi polaron could be viewed as a precursor of Nagaoka ferromagnetism. This is because, at large filling factor with increasing on-site repulsions, the impurity may leave from the short-lived repulsive polaron state at zero momentum, virtually occupy the much more well-defined super Fermi polaron state at the M point, and turn the system into the Nagaoka ferromagnetic state upon reversing its imaginable spin. We provided a thermodynamic estimation for the critical on-site repulsion U_c needed for the transition into a Nagaoka ferromagnetic state, at a given large filling factor $\nu \sim 1$. The obtained values of $U_c(\nu)$ agree qualitatively well with the previous variational calculations [11,13].

In future studies, it would be useful to improve theoretical predictions on super Fermi polarons beyond the non-self-consistent many-body T-matrix approximation. This would provide us an accurate determination of the phase diagram for the Nagaoka ferromagnetic phase transition, at both zero temperature and finite temperature. It would also motivate the experimental investigation of the intriguing Nagaoka ferromagnetism in cold-atom laboratories, by preparing a spin-population imbalanced Fermi gas in two-dimensional optical lattices [53].

ACKNOWLEDGMENTS

This research was supported by the Australian Research Council's (ARC) Discovery Program, Grants No. DP240101590 (H.H.), No. FT230100229 (J.W.), and No. DP240100248 (X.-J.L.).

APPENDIX: CHOICE OF THE BROADENING FACTOR

In Fig. 10, we report the pair propagator

$$\chi(\mathbf{q}, \omega) = \Gamma^{-1}(\mathbf{q}, \omega) - \frac{1}{U}, \tag{A1}$$

calculated at two broadening factors, $\eta = 0.1t$ (circles) and $\eta = 0.3t$ (lines), following the linear extrapolation scheme in Eq. (16). We find the results of $\chi(\mathbf{q}, \omega)$ are independent on η, except at the frequencies $\omega \sim 0$ and $\omega \sim 8t$, where its real part exhibits sharp peaks and its imaginary part starts to appear or disappear. At the small broadening factor $\eta = 0.1t$, the insufficient number of grid points used in our Gaussian quadrature integration leads to a small oscillation in the calculated pair propagator. This unwanted oscillatory behavior can be quickly removed by increasing η to $0.3t$. A nonlinear extrapolation can also be implemented to improve the numerical accuracy, but it might not be necessary, considering our purpose of clarifying the existence of super Fermi polarons.

[1] A. S. Alexandrov and J. T. Devreese, *Advances in Polaron Physics* (Springer, New York, 2010), Vol. 159.
[2] L. D. Landau, Electron motion in crystal lattices, Phys. Z. Sowjetunion **3**, 664 (1933).
[3] A. C. Hewson, *The Kondo Problem to Heavy Fermions* (Cambridge University Press, Cambridge, England, 1993).
[4] G.-M. Zhang, H. Hu, and L. Yu, Marginal fermi liquid resonance induced by a quantum magnetic impurity in d-wave superconductors, Phys. Rev. Lett. **86**, 704 (2001).
[5] I. Snyman, Structure of quasiparticles in a local Fermi liquid, Phys. Rev. B **108**, 205120 (2023).
[6] P. W. Anderson, Infrared catastrophe in fermi gases with local scattering potentials, Phys. Rev. Lett. **18**, 1049 (1967).
[7] G. D. Mahan, Excitons in metals: Infinite hole mass, Phys. Rev. **163**, 612 (1967).
[8] B. Roulet, J. Gavoret, and P. Nozières, Singularities in the X-Ray absorption and emission of metals. I. first-order parquet calculation, Phys. Rev. **178**, 1072 (1969).

[9] P. Nozières and C. T. De Dominicis, Singularities in the X-Ray absorption and emission of metals. III. one- body theory exact solution, Phys. Rev. **178**, 1097 (1969).

[10] Y. Nagaoka, Ferromagnetism in a narrow, almost half-filled *s* band, Phys. Rev. **147**, 392 (1966).

[11] B. S. Shastry, H. R. Krishnamurthy, and P. W. Anderson, Instability of the Nagaoka ferromagnetic state of the $U = \infty$ Hubbard model, Phys. Rev. B **41**, 2375 (1990).

[12] A. G. Basile and V. Elser, Stability of the ferromagnetic state with respect to a single spin flip: Variational calculations for the $U = \infty$ Hubbard model on the square lattice, Phys. Rev. B **41**, 4842(R) (1990).

[13] W. von der Linden and D. M. Edwards, Ferromagnetism in the Hubbard model, J. Phys.: Condens. Matter **3**, 4917 (1991).

[14] X. Cui and H. Zhai, Stability of a fully magnetized ferromagnetic state in repulsively interacting ultracold Fermi gases, Phys. Rev. A **81**, 041602(R) (2010).

[15] D. N. Sheng, Y. C. Chen, and Z. Y. Weng, Phase string effect in a doped antiferromagnet, Phys. Rev. Lett. **77**, 5102 (1996).

[16] F. Chevy, Universal phase diagram of a strongly interacting Fermi gas with unbalanced spin populations, Phys. Rev. A **74**, 063628 (2006).

[17] A. Schirotzek, C.-H. Wu, A. Sommer, and M. W. Zwierlein, Observation of fermi polarons in a tunable fermi liquid of ultracold atoms, Phys. Rev. Lett. **102**, 230402 (2009).

[18] Y. Zhang, W. Ong, I. Arakelyan, and J. E. Thomas, Polaron-to-Polaron transitions in the radio-frequency spectrum of a quasi-two-dimensional fermi gas, Phys. Rev. Lett. **108**, 235302 (2012).

[19] P. Massignan, M. Zaccanti, and G. M. Bruun, Polarons, dressed molecules and itinerant ferromagnetism in ultracold Fermi gases, Rep. Prog. Phys. **77**, 034401 (2014).

[20] F. Scazza, G. Valtolina, P. Massignan, A. Recati, A. Amico, A. Burchianti, C. Fort, M. Inguscio, M. Zaccanti, and G. Roati, Repulsive fermi polarons in a resonant mixture of ultracold ^{6}Li Atoms, Phys. Rev. Lett. **118**, 083602 (2017).

[21] R. Schmidt, M. Knap, D. A. Ivanov, J.-S. You, M. Cetina, and E. Demler, Universal many-body response of heavy impurities coupled to a Fermi sea: a review of recent progress, Rep. Prog. Phys. **81**, 024401 (2018).

[22] J. Wang, X.-J. Liu, and H. Hu, Exact quasiparticle properties of a heavy polaron in bcs fermi superfluids, Phys. Rev. Lett. **128**, 175301 (2022).

[23] J. Wang, X.-J. Liu, and H. Hu, Heavy polarons in ultracold atomic Fermi superfluids at the BEC-BCS crossover: Formalism and applications, Phys. Rev. A **105**, 043320 (2022).

[24] J. Wang, Functional determinant approach investigations of heavy impurity physics, AAPPS Bull. **33**, 20 (2023).

[25] M. Sidler, P. Back, O. Cotlet, A. Srivastava, T. Fink, M. Kroner, E. Demler, and A. Imamoglu, Fermi polaron-polaritons in chargetunable atomically thin semiconductors, Nat. Phys. **13**, 255 (2017).

[26] H. Hu, J. Wang, R. Lalor, and X.-J. Liu, Two-dimensional coherent spectroscopy of trion-polaritons and exciton-polaritons in atomically thin transition metal dichalcogenides, AAPPS Bull. **33**, 12 (2023).

[27] I. Bloch, J. Dalibard, and W. Zwerger, Many-body physics with ultracold gases, Rev. Mod. Phys. **80**, 885 (2008).

[28] C. Chin, R. Grimm, P. Julienne, and E. Tiesinga, Feshbach resonances in ultracold gases, Rev. Mod. Phys. **82**, 1225 (2010).

[29] P. Massignan and G. M. Bruun, Repulsive polarons and itinerant ferromagnetism in strongly polarized Fermi gases, Eur. Phys. J. D **65**, 83 (2011).

[30] Z. Yan, P. B. Patel, B. Mukherjee, R. J. Fletcher, J. Struck, and M. W. Zwierlein, Boiling a unitary fermi liquid, Phys. Rev. Lett. **122**, 093401 (2019).

[31] M. Cetina, M. Jag, R. S. Lous, I. Fritsche, J. T. M. Walraven, R. Grimm, J. Levinsen, M. M. Parish, R. Schmidt, M. Knap, and E. Demler, Ultrafast many-body interferometry of impurities coupled to a Fermi sea, Science **354**, 96 (2016).

[32] G. Ness, C. Shkedrov, Y. Florshaim, O. K. Diessel, J. von Milczewski, R. Schmidt, and Y. Sagi, Observation of a smooth polaron-molecule transition in a degenerate fermi gas, Phys. Rev. X **10**, 041019 (2020).

[33] R. Combescot, A. Recati, C. Lobo, and F. Chevy, Normal state of highly polarized fermi gases: simple many-body approaches, Phys. Rev. Lett. **98**, 180402 (2007).

[34] N. Prokof'ev and B. Svistunov, Fermi-polaron problem: Diagrammatic Monte Carlo method for divergent sign-alternating series, Phys. Rev. B **77**, 020408(R) (2008).

[35] M. M. Parish, Polaron-molecule transitions in a two-dimensional Fermi gas, Phys. Rev. A **83**, 051603(R) (2011).

[36] M. Knap, A. Shashi, Y. Nishida, A. Imambekov, D. A. Abanin, and E. Demler, Time-dependent impurity in ultracold fermions: Orthogonality catastrophe and beyond, Phys. Rev. X **2**, 041020 (2012).

[37] M. M. Parish and J. Levinsen, Highly polarized Fermi gases in two dimensions, Phys. Rev. A **87**, 033616 (2013).

[38] J. Vlietinck, J. Ryckebusch, and K. Van Houcke, Quasiparticle properties of an impurity in a Fermi gas, Phys. Rev. B **87**, 115133 (2013).

[39] S. Bour, D. Lee, H.-W. Hammer, and U.-G. Meißner, *Ab initio* lattice results for fermi polarons in two dimensions, Phys. Rev. Lett. **115**, 185301 (2015).

[40] O. Goulko, A. S. Mishchenko, N. Prokof'ev, and B. Svistunov, Dark continuum in the spectral function of the resonant Fermi polaron, Phys. Rev. A **94**, 051605(R) (2016).

[41] H. Hu, B. C. Mulkerin, J. Wang, and X.-J. Liu, Attractive Fermi polarons at nonzero temperatures with a finite impurity concentration, Phys. Rev. A **98**, 013626 (2018).

[42] H. Tajima and S. Uchino, Many Fermi polarons at nonzero temperature, New J. Phys. **20**, 073048 (2018).

[43] W. E. Liu, J. Levinsen, and M. M. Parish, Variational approach for impurity dynamics at finite temperature, Phys. Rev. Lett. **122**, 205301 (2019).

[44] J. Wang, X.-J. Liu, and H. Hu, Roton-induced bose polaron in the presence of synthetic spin-orbit coupling, Phys. Rev. Lett. **123**, 213401 (2019).

[45] H. Tajima and S. Uchino, Thermal crossover, transition, and coexistence in Fermi polaronic spectroscopies, Phys. Rev. A **99**, 063606 (2019).

[46] H. Hu and X.-J. Liu, Fermi polarons at finite temperature: Spectral function and rf spectroscopy, Phys. Rev. A **105**, 043303 (2022).

[47] H. Hu, J. Wang, J. Zhou, and X.-J. Liu, Crossover polarons in a strongly interacting Fermi superfluid, Phys. Rev. A **105**, 023317 (2022).

[48] H. Hu and X.-J. Liu, Raman spectroscopy of Fermi polarons, Phys. Rev. A **106**, 063306 (2022).

[49] H. Hu, J. Wang. and X.-J. Liu, Thermally stable *p*–wave repulsive Fermi polaron without a two-body bound state, AAPPS Bull. **33**, 27 (2023).

[50] G. E. Astrakharchik, J. Boronat, J. Casulleras, and S. Giorgini, Beyond the tonks-girardeau gas: Strongly correlated regime in quasi-one-dimensional bose gases, Phys. Rev. Lett. **95**, 190407 (2005).

[51] J. Wang, H. Hu, and X.-J. Liu, Two-dimensional spectroscopic diagnosis of quantum coherence in Fermi polarons, arXiv:2207.14509.

[52] K. Winkler, G. Thalhammer, F. Lang, R. Grimm, J. Hecker Denschlag, A. J. Daley, A. Kantian, H. P. Büchler, and P. Zoller, Repulsively bound atom pairs in an optical lattice, Nature (London) **441**, 853 (2006).

[53] A. Mazurenko, C. S. Chiu, G. Ji, M. F. Parsons, M. Kanász-Nagy, R. Schmidt, F. Grusdt, E. Demler, D. Greif, and M. Greiner, A cold-atom Fermi–Hubbard antiferromagnet, Nature (London) **545**, 462 (2017).